Bench2FreeAD: A Benchmark for Vision-based End-to-end Navigation in Unstructured Robotic Environments

Yuhang Peng, Sidong Wang, Jihaoyu Yang, Shilong Li, Han Wang and Jiangtao Gong[⊠]

Abstract-Most current end-to-end (E2E) autonomous driving algorithms are built on standard vehicles in structured transportation scenarios, lacking exploration of robot navigation for unstructured scenarios such as auxiliary roads, campus roads, and indoor settings. This paper investigates E2E robot navigation in unstructured road environments. First, we introduce two data collection pipelines - one for real-world robot data and another for synthetic data generated using the Isaac Sim simulator, which together produce an unstructured robotics navigation dataset-FreeWorld Dataset. Second, we fine-tuned an efficient E2E autonomous driving model—VAD—using our datasets to validate the performance and adaptability of E2E autonomous driving models in these environments. Results demonstrate that fine-tuning through our datasets significantly enhances the navigation potential of E2E autonomous driving models in unstructured robotic environments. Thus, this paper presents the first dataset targeting E2E robot navigation tasks in unstructured scenarios, and provides a benchmark based on visionbased E2E autonomous driving algorithms to facilitate the development of E2E navigation technology for logistics and service robots. The project is available on Github¹.

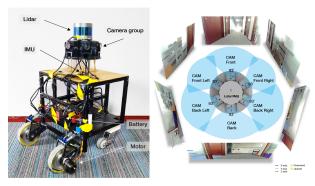


Fig. 1: Overview of the real vehicle setup, sensor coordinate system, and camera group field of view.

I. INTRODUCTION

In recent years, end-to-end (E2E) autonomous driving models have made remarkable progress, revolutionizing the field of autonomous transportation. Models such as DETR3D [1], BEVFormer [2], and UniAD [3] have

The authors are with the Institute for AI Industry Research, Tsinghua University, Beijing, China. Corresponding Email: gongjiangtao@air.tsinghua.edu.cn

demonstrated impressive capabilities in structured environments by directly mapping sensory inputs to driving actions without explicit intermediate steps. These approaches have shown particular promise in urban settings with well-defined road structures, traffic rules, and predictable agent behaviors. The VAD model [4] further advanced this field by utilizing vectorized bird's-eye view (BEV) representations, enabling more efficient real-time decision-making while maintaining high performance standards. Despite these advancements, most E2E driving models have been primarily developed and evaluated on datasets like nuScenes [5], which focus on standard high-speed vehicles in structured urban environments.

Concurrently, robot navigation technologies have evolved along several paths. Traditional approaches relied on rule-based methods such as A* and Dijkstra's algorithm [6], which perform well in controlled environments but struggle with uncertainty and dynamic scenarios. Statistical methods, including SLAM techniques [7], improved adaptability by incorporating probabilistic frameworks that better handle sensor noise and partial observability. More recently, learning-based methods have gained prominence, with Deep Reinforcement Learning (DRL)[8] enabling robots to learn complex behaviors through environmental interaction. Imitation learning approaches[9] have shown particular promise by allowing robots to mimic expert demonstrations, accelerating the acquisition of effective navigation strategies without extensive trial-and-error.

Despite these parallel advancements, autonomous navigation in unstructured environments presents persistent challenges that remain inadequately addressed. These environments—including auxiliary roads, low-speed zones, indoor spaces, and irregularly shaped pathways—lack the clear demarcations, consistent surfaces, and predictable layouts of structured settings. Navigation in such contexts requires robust handling of ambiguous boundaries, variable terrain, unexpected obstacles, and complex interactions with pedestrians and other dynamic agents. Current datasets like Replica [10], Matterport3D [11], and GOOSE [12] provide valuable resources but lack comprehensive coverage of unstructured scenarios with appropriate annotations for end-to-end autonomous navigation.

¹https://github.com/AIR-DISCOVER/FreeAD

TABLE I: COMPARISON OF DIFFERENT DATASETS

Dataset	Pose	#Cls	#3D Ann. Frames	3D Pts/Frame	2D Frames	#Sequences	Time of Day	Night/Rain	Real/Sim.	Indoor/Outdoor	Map layers	Map nums
KITTI	G+R	3	15K	120K	13K	22	M, A	N/N	Y/N	Outdoor only	-	_
nuScenes	G+R	23	40K	34K	1.4M	1000	M, A, E	Y/Y	Y/N	Outdoor only	11	4
CODa	S+G	53	32K	131K	131K	54	M, A, E	Y/Y	Y/N	Outdoor/Indoor	-	_
JRDB	None	1	28K	130K	28K	_	M, A	N/N	Y/N	Outdoor/Indoor	-	_
SCAND	None	0	0	65K	626K	_	M, A	N/N	Y/N	Outdoor/Indoor	-	_
Free World	G+R	1	2K	4.4K	32K	50	M, A	N/N	Y/Y	Indoor/Outdoor	1	5

In this paper, we address these challenges by developing a comprehensive approach to E2E robot navigation in unstructured environments. We introduce two complementary data collection pipelines: one gathering realworld robot navigation data across various unstructured settings, and another generating synthetic data using the Isaac Sim simulation environment. These pipelines yield a rich, diverse dataset specifically designed for training and evaluating navigation models in unstructured scenarios. Our dataset features annotations of road dividers as the primary static object class (with all other areas considered navigable) and 3D bounding boxes for dynamic objects, particularly pedestrians.

Building on this dataset, we fine-tune the VAD model [4] for unstructured environment navigation. This adaptation process involves adjusting the model architecture to better handle the unique characteristics of unstructured environments while maintaining computational efficiency for deployment on resource-constrained robot platforms. Our fine-tuning methodology balances performance enhancement with generalization capabilities, ensuring the model functions effectively across a range of previously unseen unstructured scenarios.

The contributions of this work are threefold:

- We present the first comprehensive dataset specifically designed for E2E robot navigation in unstructured environments, featuring both real-world and synthetic data with appropriate annotations for static and dynamic objects.
- We demonstrate the successful adaptation of the VAD model to unstructured navigation contexts through a specialized fine-tuning process, significantly enhancing its performance in these challenging scenarios.
- We establish a benchmark for vision-based E2E autonomous navigation in unstructured environments, providing a foundation for future research in this emerging field and facilitating the development of navigation technologies for logistics and service robots.

II. THE FREEWORLD DATASET

A. Whole Dataset

We collected over 2,000 samples in just three hours—covering five maps with vector annotations across 50 scenes—and annotated more than 2,000 3D bounding boxes. An example is shown in Fig. 2.

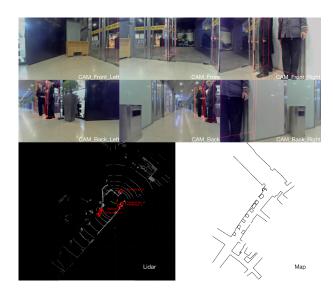


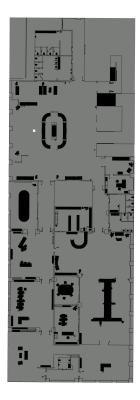
Fig. 2: An example from the FreeWorld dataset. We see 6 different camera views and lidar data, as well as the human annotated semantic map. At the bottom we show the human written scene description.

B. Benchmark

We use a different benchmark for map definition compared to the nuScenes dataset, as our environment is unstructured. Instead of following the structured mapping approach used in MapTR [13], we model the ground truth (GT) map using a simplified semantic layer that focuses primarily on road dividers. Although we initially experimented with the incorporation of both boundaries and dividers in Fig. 4, we found that it was unnecessary. Road dividers serve as representations of boundaries and static obstacles that cannot be traversed. All other areas are considered navigable. We believe that reducing the emphasis on semantic segmentation will help the model focus more on obstacle detection and learn their general characteristics. Additionally, due to the scarcity of dynamic objects in our less transportation-focused, unstructured environment, we annotate only one class of 3D bounding boxes: humans. These 3D boxes represent dynamic obstacles that should be avoided.

C. Robot Setup

1) Real World: We employ a custom-built small robot, with the sensor layout illustrated in Fig. 1 and detailed specifications provided in Table II, Unlike



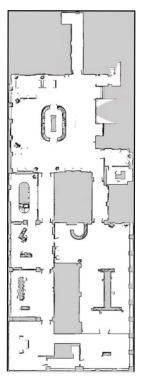


Fig. 3: Comparison of Occupancy Generator and SLAM Mapping. The occupancy generator produces a map with finer details and higher precision compared to the SLAM mapping approach.

nuScenes, our LiDAR coordinates align with the ego frame.. The sensors are securely mounted using a custom designed module (shown in Fig. 1) to ensure stable and precise positioning. Each of the six cameras is equipped with a horizontal field of view (HFOV) of 93 ° and a vertical field of view (VFOV) of 61 °. This wide field of view allows the robot to capture a more comprehensive perspective at close distances, ensuring adequate overlap between the views of different cameras, as shown in Fig. 1. In contrast to outdoor vehicles, which typically possess longer detection ranges, the cameras in our robot are specifically optimized for close-range, high-resolution observation.

2) Isaac Sim: In the Isaac Sim environment, the sensor group is placed atop a human model, with the sensors configured as child objects of the model to follow its movement. All six cameras and the LiDAR sensor are positioned at the same location, eliminating the need for extrinsic calibration and simplifying the setup.

Sensor Type	Specifications				
	6x Camera RGB				
	7Hz capture frequency				
	1/2.5" IMX274 sensor				
Camera	HFOV: 93°				
	VFOV: 61°				
	1920×1080 resolution,				
	auto exposure, JPEG compressed				
	1x Lidar Spinning, 16 beams				
	20Hz capture frequency				
Lidar	360° horizontal FOV				
Liuai	-15° to 15° vertical FOV				
	\leq 150m range, \pm 2cm accuracy,				
	up to 300k points per second				
	IMU, HI229				
IMU	10° heading, 0.8° roll/pitch				
	400Hz update rate				

TABLE II: Sensor specifications in the real world

D. Sensor Synchronization

In the real-world robot setup, we use the ROS2 Approximate Time Synchronizer to align sensor data, filtering out measurements with time differences exceeding 0.2s. In contrast, Isaac Sim operates with a lower frame capture rate, reducing the data acquisition burden. Therefore, we use ExactTime synchronization, discarding frames with any time discrepancies to ensure precise alignment between each image and its corresponding 3D bounding box annotations.

E. Imitation Behavior

In our real-world setup, the robot is operated via remote control, allowing the driver to navigate to designated locations while skillfully avoiding obstacles such as pedestrians. This process generates valuable data on navigation behavior. In Isaac Sim, the predefined data acquisition path is shown in Fig. 4, while the character's walking path is similarly rendered. We utilize a navmesh-based navigation system with set waypoints to ensure that the robot reaches its target while effectively avoiding human figures, ultimately producing high-quality expert navigation data.

F. Localization

In the real-world setup, we use a SLAM algorithm to fuse data from motor encoders and LiDAR point clouds for localization, as GPS is unavailable indoors and no map is available. During data collection, we also apply a Monte Carlo Localization method based on LiDAR and odometry information, which is highly robust and achieves localization errors of less than 10 cm. In Isaac Sim, we rely on the TF data provided by the simulation environment to obtain positional information.

G. Maps

In the real world, we use a SLAM algorithm for map creation. In Isaac Sim, we employ grid maps generated by the occupancy generator. Notably, we also perform SLAM-based mapping within the simulation environment. We have observed that maps generated by the occupancy generator tend to be more detailed and richer due to its highly controlled algorithm, as shown in Fig. 3. In contrast, the LiDAR-based SLAM approach is limited by the sensor's accuracy.

H. Data Annotation

In the real world, we use the tool described in [14] to annotate LiDAR and image data together with 3D bounding boxes, enhancing the accuracy and reference quality of the annotations. In Isaac Sim, we use the built-in Camera Helper to output 3D bounding boxes for annotation.

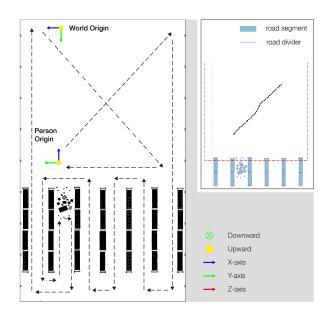


Fig. 4: Visualization of the data acquisition process in Isaac Sim and the ego pose in the first scene of the *Full Warehouse* map. The left image illustrates the data acquisition path, while the right image shows the ego pose rendered with two map layers: *road divider* and *road segment*.

III. METRICS

A. Detection Task

FreeWorld detects humans using 3D bounding boxes, attributes (e.g., sitting/standing), and velocity vectors, and maps road dividers in real time.

1) Average Precision: We adopt the Average Precision (AP) metric with a twist: matches are based on the 2D center distance d on the ground plane instead of IoU. This decouples detection accuracy from object size and orientation, making comparisons with vision-only methods fairer. AP is computed as the normalized

area under the precision-recall curve, considering only operating points where both recall and precision exceed 10%. If none exist, AP is zero.

B. Tracking Task

1) L2 Error: The L2 error is the mean Euclidean distance between predicted and ground truth trajectories over T steps:

L2 Error =
$$\frac{1}{T} \sum_{t=1}^{T} \| \tau_t - \tau_t^{\text{gt}} \|_2$$
.

2) Collision Rate: Collision rate quantifies how often the planned trajectory intersects obstacles. At each step, the vehicle's polygonal footprint is projected onto the BEV map. A collision is flagged if any pixel overlaps an obstacle. For N trajectories, it is defined as:

Collision Rate =
$$\frac{1}{N} \sum_{i=1}^{N} \sum_{t=1}^{T} \mathbb{1} \left(\text{collision}_{i,t} \right),$$

where $\mathbb{1}(\cdot) = 1$ if a collision occurs, and 0 otherwise.

3) Average Displacement Error (ADE): The Average Displacement Error (ADE) measures the average Euclidean distance between predicted trajectories and the ground truth trajectories across all time steps. It is defined as:

$$ADE = \frac{1}{T} \sum_{t=1}^{T} ||\hat{y}_t - y_t||$$

Where:

- T is the total number of time steps.
- \hat{y}_t is the predicted position at time step t.
- y_t is the ground truth position at time step t.
- 4) Final Displacement Error (FDE): The Final Displacement Error (FDE) measures the Euclidean distance between the predicted trajectory's final position and the ground truth's final position. It is defined as:

$$FDE = \|\hat{y}_T - y_T\|$$

Where:

- T is the total number of time steps.
- \hat{y}_T is the predicted final position.
- y_T is the ground truth final position.

IV. EXPERIMENTS

A. Implementation Details

We conducted experiments on the FreeWorld dataset, which comprises 50 unstructured road scenes, each lasting approximately 20 seconds. The dataset contains a total of 3.8k 3D bounding boxes for a single category. Scene images are captured using six cameras that provide a 360° horizontal field of view, with keyframes

TABLE III: Open-loop Results on FreeWorld: Comparison of VAD-Tiny, VAD-Base, and FT-VAD under the "Divider Only" map modeling strategy. ADE and FDE represent pedestrian motion prediction errors.

Method	L2 (m) ↓				AP divider ↑	FPS ↑	Collision (Avg. %)	ADE ↓	FDE ↓
	1s	2s	3s	Avg.					
VAD-Tiny	0.891	1.600	2.449	1.647	0.000	8.7	0.00	2.848	3.294
VAD-Base	0.499	0.759	1.040	0.766	0.001	5.0	0.00	2.089	2.917
FT-VAD	0.421	0.596	0.760	0.592	0.567	5.0	0.00	1.432	2.319

AP divider is computed with a threshold of 1.5.

annotated at a frequency of 2 Hz. Following previous research [4], we evaluate planning performance using displacement error (DE), composition error AP in the divider, and collision rate (CR) across different Models and datasets. These metrics offer a comprehensive assessment of planning accuracy and safety.

FT-VAD is our variant of the VAD-Base model that was fine-tuned on the FreeWorld dataset over two stages—6 epochs in Stage 1 and 3 epochs in Stage 2—resulting in enhanced performance in unstructured environments.

We used three A100 GPUs for training and fine-tuning the models, and one A100 GPU was used for inference evaluation.

B. Main Results

We evaluated three models—VAD-Tiny, VAD-Base, and FT-VAD-across the FreeWorld and nuScenes datasets. To mimic the nuScenes configuration, we defined a map layer incorporating both boundary and divider elements. However, our results indicate that including the boundary layer degrades detection performance and reduces FPS compared to using the divider alone. Consequently, for unstructured environments we adopt the divider-only map, which yields higher prediction accuracy and faster inference. Moreover, as shown in Fig. 6, although VAD captures the overall shape of a boundary, it significantly overestimates its distance—predicting it to be over 3 meters away when the true distance is less than 50 cm. This suggests that VAD is more suitable for autonomous driving on structured roads.

For the divider-only map in FreeWorld (see Table III), FT-VAD achieved the lowest L2 error (0.592 m), outperforming VAD-Base (0.766 m) and VAD-Tiny (1.647 m). While VAD-Base's cautious, slower behavior reduces trajectory deviation, FT-VAD markedly improves the AP divider metric (0.567 vs. 0.001/0.000), indicating superior map composition in unstructured scenes. Inference speeds were comparable—FT-VAD and VAD-Base at 5 FPS, and VAD-Tiny at 8.7 FPS—with all models recording zero collisions due to the sparse dynamic obstacles and low operating speeds.In addition to its improved L2 performance, FT-VAD also demonstrated superior

pedestrian motion prediction accuracy, achieving the lowest ADE (1.432) and FDE (2.319), outperforming VAD-Base (ADE: 2.089, FDE: 2.917) and VAD-Tiny (ADE: 2.848, FDE: 3.294). This suggests FT-VAD's enhanced ability to predict motion paths with greater precision.

In contrast, on the nuScenes dataset (see Table IV), VAD-Tiny and VAD-Base maintained low L2 errors (approximately 0.76 m and 0.70 m, respectively at 2s), while FT-VAD exhibited substantially higher errors (approximately 3.24 m at 2s and 4.38 m at 3s). Fine-tuned on FreeWorld, FT-VAD's low-speed strategy is less effective on structured, high-speed roads and may suffer from catastrophic forgetting during task transfer; its low collision rate primarily stems from its conservative speed.

TABLE IV: Open-loop L2 and Collision Rates Comparison for Different Models on the nuScenes Dataset

Method]	L2 (m)	 	Collision (%) ↓			
	1s	2s	3s	1s	2s	3s	
VAD-Tiny	0.46	0.76	1.12	0.21	0.35	0.58	
VAD-Base	0.41	0.70	1.05	0.07	0.17	0.41	
FT-VAD	2.02	3.24	4.38	0.00	0.00019	0.00016	

C. Analysis

The displacement error (DE) shows significant differences between the Models, likely due to the fact that low-speed robots navigate unstructured environments, while high-speed vehicles operate in structured settings. Moreover, the collision rate (CR) remains nearly zero because of the limited presence of pedestrians in both indoor and outdoor scenarios—even in densely populated datasets such as nuScenes. However, we contend that CR is not a suitable metric for our approach, given that the lower operating speeds of our robots inherently decrease the likelihood of collisions.

Furthermore, the elevated L2 errors observed for FT-VAD on the nuScenes dataset may also be partially explained by catastrophic forgetting during task transfer. Fine-tuned on the FreeWorld dataset, FT-VAD learns a low-speed strategy that works well in unstructured environments but does not generalize to the higher-speed, structured scenarios of nuScenes. This obser-



Fig. 5: Qualitative results of FreeAD. FreeAD generates vectorized representations of unstructured scenes and predicts 3D bounding boxes for people.



Fig. 6: Qualitative results of VAD on the FreeWorld dataset.

vation further emphasizes the fundamental differences between tasks in unstructured environments and those on structured roads. Moreover, differences in mapping modeling—stemming from the distinct environmental representations and mapping approaches used in each dataset—also contribute to these performance disparities.

D. Qualitative Results

We show three vectorized scene learning and planning results of FreeAD in Fig. 5 and VAD results in Fig.6. For a better understanding of the scene, we also provide raw surrounding camera images

V. CONCLUSIONS AND FUTURE WORK

In this paper, we explored end-to-end robot navigation in unstructured road environments. Our results demonstrate that the fine-tuned VAD model exhibits significant potential and robust performance in these challenging scenarios. Furthermore, we established efficient data collection pipelines for both real-world robots and simulation platforms, successfully gathering diverse datasets that will facilitate future data-driven approaches to navigation in unstructured settings. These datasets provide valuable resources for enhancing model accuracy and adaptability.

Looking ahead, our future work will concentrate on further improving model robustness and global target navigation capabilities. We also plan to investigate the integration of world models [15] to advance autonomous navigation technologies in complex environments. Additionally, we aim to expand the scale and diversity of the FreeWorld Dataset and incorporate closed-loop training and evaluation protocols, such as those presented in Bench2Drive [16], to further refine our approach.

ACKNOWLEDGMENT

This research is supported by the National Natural Science Foundation Youth Fund 62202267, Beijing Municipal Science and Technology Project (Nos. Z231100010323005), and Beijing Natural Science Foundation (Grant No.L233033).

APPENDIX

REFERENCES

- [1] Y. Wang, V. C. Guizilini, T. Zhang, Y. Wang, H. Zhao, and J. Solomon, "Detr3d: 3d object detection from multi-view images via 3d-to-2d queries," in *Conference on Robot Learning*. PMLR, 2022, pp. 180–191.
- [2] Z. Li, W. Wang, H. Li, E. Xie, C. Sima, T. Lu, Q. Yu, and J. Dai, "Bevformer: learning bird's-eye-view representation from lidarcamera via spatiotemporal transformers," *IEEE Transactions on Pattern Analysis and Machine Intelligence*, 2024.

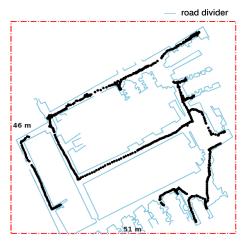


Fig. 7: Visualization of ego poses in the *RealWorld Map*

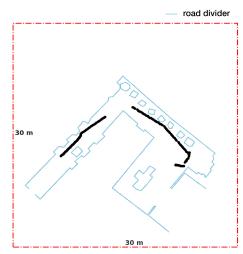


Fig. 8: Visualization of ego poses in the *RealWorld Map*

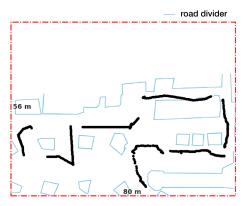


Fig. 9: Visualization of ego poses in the *RealWorld Map* 3

- [3] Y. Hu, J. Yang, L. Chen, K. Li, C. Sima, X. Zhu, S. Chai, S. Du, T. Lin, W. Wang, et al., "Planning-oriented autonomous driving," in Proceedings of the IEEE/CVF conference on computer vision and pattern recognition, 2023, pp. 17853–17862.
- [4] B. Jiang, S. Chen, Q. Xu, B. Liao, J. Chen, H. Zhou, Q. Zhang, W. Liu, C. Huang, and X. Wang, "Vad: Vectorized scene representation for efficient autonomous driving," in *Proceedings of the IEEE/CVF International Conference on Computer Vision*, 2023, pp. 8340–8350.
- [5] H. Caesar, V. Bankiti, A. H. Lang, S. Vora, V. E. Liong, Q. Xu, A. Krishnan, Y. Pan, G. Baldan, and O. Beijbom, "nuscenes: A multimodal dataset for autonomous driving," in *Proceedings of the IEEE/CVF conference on computer vision and pattern recognition*, 2020, pp. 11621–11631.
- [6] X. Xiao, B. Liu, G. Warnell, and P. Stone, "Motion planning and control for mobile robot navigation using machine learning: a survey," *Autonomous Robots*, vol. 46, no. 5, pp. 569–597, 2022.
- [7] S. Macenski and I. Jambrecic, "Slam toolbox: Slam for the dynamic world," *Journal of Open Source Software*, vol. 6, no. 61, p. 2783, 2021.
- [8] K. Zhu and T. Zhang, "Deep reinforcement learning based mobile robot navigation: A review," *Tsinghua Science and Tech*nology, vol. 26, no. 5, pp. 674–691, 2021.
- [9] A. Hussein, M. M. Gaber, E. Elyan, and C. Jayne, "Imitation learning: A survey of learning methods," ACM Computing Surveys (CSUR), vol. 50, no. 2, pp. 1–35, 2017.
- [10] J. Straub, T. Whelan, L. Ma, Y. Chen, E. Wijmans, S. Green, J. J. Engel, R. Mur-Artal, C. Ren, S. Verma, et al., "The replica dataset: A digital replica of indoor spaces," arXiv preprint arXiv:1906.05797, 2019.
- [11] A. Chang, A. Dai, T. Funkhouser, M. Halber, M. Niessner, M. Savva, S. Song, A. Zeng, and Y. Zhang, "Matterport3d: Learning from rgb-d data in indoor environments," arXiv preprint arXiv:1709.06158, 2017.
- [12] P. Mortimer, R. Hagmanns, M. Granero, T. Luettel, J. Petereit, and H.-J. Wuensche, "The goose dataset for perception in unstructured environments," in 2024 IEEE International Conference on Robotics and Automation (ICRA). IEEE, 2024, pp. 14838–14844.
- [13] B. Liao, S. Chen, X. Wang, T. Cheng, Q. Zhang, W. Liu, and C. Huang, "Maptr: Structured modeling and learning for online vectorized hd map construction," arXiv preprint arXiv:2208.14437, 2022.
- [14] E. Li, S. Wang, C. Li, D. Li, X. Wu, and Q. Hao, "Sustech points: A portable 3d point cloud interactive annotation platform system," in 2020 IEEE Intelligent Vehicles Symposium (IV). IEEE, 2020, pp. 1108–1115.
- [15] X. Wang, Z. Zhu, G. Huang, X. Chen, J. Zhu, and J. Lu, "Drive-dreamer: Towards real-world-drive world models for autonomous driving," in *European Conference on Computer Vision*. Springer, 2024, pp. 55–72.
- [16] X. Jia, Z. Yang, Q. Li, Z. Zhang, and J. Yan, "Bench2drive: Towards multi-ability benchmarking of closed-loop end-to-end autonomous driving," arXiv preprint arXiv:2406.03877, 2024.